Bull. Chem. Soc. Ethiop. **2024**, 38(6), 1897-1914.
DOI: https://dx.doi.org/10.4314/bcse.v38i6.30

ISSN 1011-3924
Printed in Ethiopia
Online ISSN 1726-801X

UNVEILING THE NOVEL ANTI-CORROSION AND ANTI-BACTERIAL BIOFILM FORMING CHARACTERISTICS OF ECO-SAFE MWCNT-AZ91E ALLOY FOR FOOD-PROCESSING SURFACES

Veera Prabakaran Elanjeitsenni* and Senthil Vadivu Kulandhaivelu

Department of Printing and Packaging Technology, College of Engineering Guindy, Anna University, Chennai, 600025, India

(Received May 11, 2024; Revised July 1, 2024; Accepted July 11, 2024)

ABSTRACT. This study explores the eco-friendly modification of AZ91E alloy with MWCNT casting to enhance surfaces crucial for food processing, storage, and transportation, with a specific focus on reducing bacterial biofilm formation and preventing corrosion. Incorporating nanomaterials like MWCNT into magnesium alloys offers promising prospects for improving the surfaces of equipment and structures used in food-related industries. The advanced mechanical properties observed in MWCNT-doped alloys can lead to the development of lightweight yet durable surfaces essential for maintaining hygiene standards and ensuring food safety during processing, storage, and transportation. Employing sophisticated systematic practices such as XRD, FTIR, and Vickers hardness testing allows for comprehensive evaluation of surface modifications and mechanical enhancements. Furthermore, the demonstrated corrosion resistance of MWCNT-doped magnesium alloys is crucial for protecting surfaces from degradation caused by exposure to corrosive environments commonly encountered in food processing facilities and transportation systems. Additionally, the remarkable antibacterial properties exhibited by MWCNT-doped alloys hold promise for mitigating bacterial biofilm formation on surfaces, thereby contributing to enhanced sanitation and hygiene practices in food-related industries.

KEY WORDS: Multiwalled carbon nanotube, Magnesium alloys, Anticorrosion, Squeeze casting, Antibacterial, Biofouling

INTRODUCTION

Biofouling is another critical issue that impacts the performance of magnesium alloys in the food industry which refers to the accumulation of microorganisms, such as bacteria, algae, and fungi, as well as organic matter, on the surface of materials. In food storage and transportation applications, biofouling can occur due to the presence of food residues, organic contaminants, and microbial growth, leading to corrosion and degradation of the alloy surface. Moreover, biofouling can create harborage sites for pathogens and spoilage organisms, further compromising food safety. These challenges highlight the need for effective solutions to augment the corrosion confrontation and biofouling resistance of magnesium (Mg) alloys in food-related applications. While magnesium alloys offer many advantages, their susceptibility to corrosion and biofouling limits their potential use in critical food-handling processes. Addressing these challenges requires innovative approaches that not only mitigate corrosion and biofouling but also maintain high standards of food safety and product integrity.

Magnesium and its alloys possess the lowest density of all structural metallic materials with the blend of exceptional engineering characteristics, including low density, low inherent stiffness, favourable biocompatibility, outstanding castability, and a high potential for recycling [1]. These materials can be manufactured using various methods and are highly suitable for wide range of applications. A significant application of these alloys is to be utilised in food transportation and storage applications where weight reduction is a priority, such as in the construction of lightweight pallets or containers used for transporting perishable goods [2]. Substituting aluminium with magnesium results in weight reduction due to the lower density of pure magnesium (1.8 g/cm^3)

*Corresponding authors. E-mail: veeraprabakaran.india@gmail.com

compared to pure aluminium (2.7 g/cm^3) [3]. However, their susceptibility to corrosion and biofouling has limited their widespread adoption in these critical areas. Corrosion, caused by exposure to various environmental factors such as moisture, acids, and salts, poses a significant challenge to magnesium alloys, leading to degradation of structural integrity and potential contamination of food products. Additionally, biofouling, the accumulation of microorganisms and organic matter on surfaces, further exacerbates corrosion issues and compromises food safety [4]. Corrosion can lead to the degradation of the alloy's surface, compromising its structural integrity and potentially contaminating food products. This poses a serious risk to food safety and can result in product recalls, financial losses, and environmental safety [5]. Structural failures resulting from corrosion can threaten human life and the environment, especially in critical infrastructure systems. Corrosion products from magnesium alloys can leach into the surrounding soil and water bodies, contaminating terrestrial and aquatic ecosystems. This contamination may adversely affect soil fertility, water quality, and marine life, disrupting natural habitats and potentially harming plant and animal species. The corrosion confrontation of Mg-Al alloys is influenced by the presence of impurity elements that function as active cathodes and the microstructure [6]. The study of magnesium's behaviour in different environments has been a significant area of research for chemists and materials scientists [7]. These investigations primarily aimed to enhance the chemical and electrochemical behaviour of magnesium and its alloys under various situations, offering suitable ways to address the problem. Multiple techniques, such as surface treatment, surface coating, and the accumulation of alloying rudiments, can be employed to reduce the chemical reactivity of magnesium alloys in different hostile environments [8]. Surface coating on magnesium alloys often improves corrosion resistance, enhances wear properties, or provides decorative finishes. However, surface coating may present certain drawbacks during application and use despite its advantages. Proper adhesion between the coating and the magnesium alloy substrate can be challenging as its low surface energy and high chemical reactivity can hinder adhesion, leading to poor coating adhesion, delamination, and premature failure, particularly in aggressive environments or under mechanical stress.

Coatings applied to magnesium alloys may experience cracking, porosity, or pinhole formation during application or service conditions. Factors such as thermal expansion mismatches between the coating and substrate, moisture ingress, or mechanical stress can induce coating defects, compromising corrosion resistance and exposing the underlying substrate to degradation. The casting processes ensure uniform corrosion protection across the entire component. The corrosion confrontation of Mg alloy is integrated into the structure, providing consistent protection even in areas that are difficult to access or coat effectively. Casting components with magnesium alloys can be more environmentally friendly than surface coating methods. Surface coatings may involve chemicals, solvents, and volatile organic compounds (VOCs), which pose environmental and health risks during application, handling, and disposal [9]. Casting magnesium alloys eliminates the need for these potentially hazardous substances, reducing environmental impact and ensuring safer working conditions. Remarkably, various nanomaterials have been employed to advance the corrosion fortification of Mg alloys. Nanomaterials can adhere more effectively to the surface of magnesium alloys than conventional coatings. Their small size allows them to penetrate surface irregularities and form strong bonds with the substrate, ensuring long-lasting adhesion and durability of the corrosion protection layer. Incorporating nanomaterials into magnesium alloys can also improve their mechanical properties, such as strength, hardness, and toughness. This dual functionality allows for producing corrosion-resistant components that meet stringent mechanical requirements, making them suitable for demanding applications in harsh environments.

Numerous nanomaterials and nanocomposites, such as zinc (Zn), strontium (Sr), silicon carbide (SiC), lanthanum (La), and graphene, have been employed to enhance corrosion inhibition, reduce grain size, improve dissolved oxygen levels, and enhance overall mechanical

properties [10]. Among these, multi-walled carbon nanotubes (MWCNTs) represent a distinct class of nanomaterials with exceptional physical, chemical, and mechanical attributes, rendering them versatile across a spectrum of disciplines, including materials science, electronics, energy storage, biomedical engineering, and environmental remediation. Integrating MWCNTs into magnesium alloy matrices confers a reinforcing effect, augmenting the alloy's mechanical characteristics such as tensile strength, hardness, and modulus of elasticity. Leveraging their remarkable mechanical strength and stiffness, MWCNTs function as efficacious reinforcing agents, adept at resisting deformation and fortifying load-bearing capacity [11]. Furthermore, while magnesium alloys are renowned for their high specific strength, they may exhibit constrained ductility and toughness, particularly at ambient temperatures. Incorporating MWCNTs mitigates this limitation by fostering homogeneous deformation and facilitating energy absorption mechanisms, culminating in enhanced fracture toughness and impact resistance within the composite material.

This study addressed to advancing MWCNT-reinforced magnesium alloy (AZ91E) by employing the stir squeeze technique to achieve homogeneous particle dispersion for their anticorrosion and antibacterial applications. A comprehensive examination of the structural, mechanical, and corrosion properties has been undertaken to ensure significant material performance and functionality enhancements. Through meticulous investigation, this research endeavours to propel the development of innovative materials with superior characteristics, catering to diverse industrial applications and addressing pertinent engineering challenges.

EXPERIMENTAL

Materials

The AZ91E Mg alloy obtained from Exclusive Magnesium Pvt. Ltd in India was used as the primary material for creating the composite in this study. The reinforcing agent selected for this study was MWCNTs obtained from Sigma Aldrich. The diameters of these MWCNTs range from 40 to 60 nm in diameter and from 5 to 10 μm in size.

Fabrication process of MWCNT-AZ91E

The composite fabrication process utilised a state-of-the-art UST-assisted stir squeeze casting technique, employing equipment sourced from Swam Equip in India. The procedure commenced by preheating the furnace to 800°C, then introducing 1 kg of AZ91E magnesium alloy, with continuous temperature monitoring facilitated by a thermocouple. To mitigate the flammability of magnesium, the melting process was conducted under an inert gas blend comprising 90% Argon and 10% SF6. A mechanical stirrer, operating at 450 rpm, ensured the consistent melting of the alloy. Preheated MWCNT powder was incorporated through an integrated vibrator, followed by meticulous stirring to attain uniform dispersion [8]. Ultrasonic waves were introduced into the melt via a 2500 W, 20 kHz transducer coupled with an acoustic generator, applied for 15 min. Subsequently, the molten metal, maintained at 720 °C, was poured from the bottom into a preheated split-type squeeze die (φ50 x l300 mm) maintained at 300 °C. The final stage involved applying a squeeze pressure of 120 MPa for 1 min to solidify the composite and the produced composite sample is designated as A-MWCNT [4].

Antibacterial activity

From National Chemical Laboratory in Pune, India, we procured the Gram-negative *E. coli* and the Gram-positive *Staphylococcus aureus*. The specimen organisms were incubated at 37 °C for 12 to 15 hours after being put in a nutrient broth to start the bacterial growth process. The growth

and multiplication of the bacteria in the liquid was accompanied by an obvious rise in turbidity. The antibacterial characteristics of the A-MWCNT and AZ91E alloy were tested using the outstanding diffusion approach. The Muller-Hinton agar (MHA) process was used to make the alloy. The bacterial cultures were transferred on petri plates that had already been treated with MHA. The test samples were prepared by meticulously grinding and scratching off A-MWCNT and AZ91E alloys at 25, 50, and 75 mg/mL concentrations. Also, a control stent made of S 25 material was used. A 6 mm diameter well was bored into the Petri dish, and a micropipette with a calibrated concentration of nanoparticles and a control material was inserted into it. To ensure the bacteria could thrive in an aerobic environment, the culture was then incubated at 37 °C for 24 hours. We measured the inhibition area that developed around the test materials to determine their efficacy against bacteria.

Characterization techniques

The XRD patterns of A-MWCNT and AZ91E specimens were acquired employing a Philips X'Pert MPD powder diffractometer. This equipment, developed by PANalytical in the Netherlands, was configured with an extended narrow focus of a copper anode operating at 40 kV and 30. The FTIR was conducted using a Spectrum 100 apparatus from PerkinElmer, Shelton, CT, to analyse the functional groups present. The prepared samples were varied with KBr and compressed into bits by means of a hydraulic press. Subsequently, the pellets underwent FTIR spectroscopy across the wavenumber range of 4000 to 400 cm^{-1}. The morphological characteristics of the materials were examined using a SEM, X Flash 7, Bruker. The hardness of the specimens was evaluated via Vickers hardness testing in which diamond pyramid indenter with a square base was utilised by applying a force of 500 grams for 15 seconds. The specimens were secured, and the lenses were adjusted to obtain sharp images at the optimal focal length. Indentations were made according to predetermined criteria to ensure proper alignment and placement of measurement lines at two diagonally opposite corners. Measurements were taken at five locations, and the mean hardness was determined. Furthermore, the hardness (H) and reduced modulus (Er) of the prepared alloy samples were measured and the measuring instrument was calibrated using fused quartz as a reference sample. Indentation testing was conducted at three locations on each sample using a force of 1900 μN. A piezo automation setup was employed in click script mode to streamline the testing procedure. Each indentation cycle comprised a 15-second loading and unloading time, with a 5-second interval between cycles. Using the obtained indentation data, the quasi-static analysis program automatically computed the specimens' hardness and elastic modulus. The EIS was used to evaluate the corrosion behaviour of prepared A-MWCNT and AZ91E samples which are conducted at room temperature using an electrochemical workstation (PGSTAT302N; Metrohm Autolab, Netherlands).

Estimation of anticorrosion

The experimental procedure commenced with meticulously cleaning the plate surfaces using ethanol and deionised water, ensuring the removal of any extraneous impurities adhering to the surface. Subsequently, the plates were precisely cut into dimensions measuring 100 x 1 x 1 mm. Following preparation, the plates were immersed in various hydrochloric acid (HCl) electrolyte concentrations. The electrochemical corrosion analysis was conducted utilising electrochemical impedance spectroscopy (EIS) autolab instrumentation. Specifically, the study involved the utilisation of AZ91E and ACNT configurations as functional electrodes, with Ag/AgCl as the reference and platinum as counter electrode. The test plates were employed as the working electrode during the experimental assessment.

RESULTS AND DISCUSSION

Crystallographic and microstructural analysis

Figure 1(a) depicts the XRD spectrum obtained for prepared A-MWCNT and AZ91E samples. The predominant peaks of magnesium alloy were observed at the 2θ positions 32.77°, 34.95°, 37.20°, 48.43°, 58.05°, 63.69°, 69.31°, 70.37° and 72.73°. The observed 2θ positions can be attributed to the crystal planes of forming Mg and the secondary phase of Mg17Al12. The doping mixture of MWCNT in sample A-MWCNT can be observed through the presence of additional peaks formed at the 2θ positions 25.98° and 42.28° which can be attributed to the carbon peaks of MWCNT having crystal planes (002) and (100), respectively. Additionally, there is a significant reduction in the secondary phase formed $Mg_{17}Al_{12,}$ resulting in the overall structural stability of the prepared samples. Additionally, the crystalline size of prepared samples was assessed using Debye Scherrer equivalence [12]:

$$D = \frac{k\lambda}{\beta\, cos\theta} \tag{1}$$

where, the average crystalline size is represented as D, the wavelength of the source used is described as λ (1.5406 Å), k is the shape factor (0.9), β is the FWHM diffraction peak, and θ is the Bragg slant. The average D spacing (Å), average crystalline size, dislocation density (δ × 1015 lines/m^2) and microstrain of the AZ91E are 1.84, 39.98, 0.626 and 2.33 whereas MWCNT exhibited 1.91, 34.61, 0.835 and 2.79, respectively. It is observed there is a significant increase in the microstrain of A-MWCNT when compared to AZ91E samples. The increase in dislocation density in MWCNT cast AZ91E Mg alloy can be ascribed to the incorporation of MWCNTs during the casting process. When MWCNTs are added to the magnesium alloy matrix, they introduce lattice defects and imperfections due to the differences in crystal structure and lattice parameters between the MWCNTs and the magnesium matrix. Throughout the solidifying progression of the alloy, the presence of MWCNTs disrupts the regular atomic arrangement, leading to the formation of dislocations in the crystal lattice. These dislocations act as defects in the crystal structure, creating regions of higher strain and stress within the material when the dislocation density increases, reflecting the concentration of these lattice defects per unit volume of the alloy. Further, the crystalline size of the A-MWCNT sample is comparatively lower than the AZ91E samples. This can be attributed to the influence of MWCNT acting as effective nucleation sites for forming new grains during the solidification process. As the molten magnesium alloy cools and solidifies around the MWCNTs, they can promote the formation of smaller crystalline grains compared to the absence of MWCNTs. This nucleation effect results in a finer microstructure and a decrease in the average crystalline size of the composite material. Additionally, MWCNTs can hinder crystalline grains' growth during solidification. As the alloy cools, the MWCNTs dispersed within the matrix can impede the movement and coalescence of individual grains, limiting their growth to smaller sizes. This effect prevents the formation of larger crystalline grains and contributes to a reduction in the overall crystalline size of the composite material.

The dislocation density (δ) of prepared samples is determined by measuring the span of displacement appearances per unit volume of the crystal (Equation 3):

$$\delta = \frac{1}{D^2} \tag{2}$$

Similarly, the microstrain (ε_{hkl}) of prepared A-MWCNT and AZ91E samples was estimated using the following equation [14]:

$$\varepsilon = \frac{\beta cos\theta}{4} \tag{3}$$

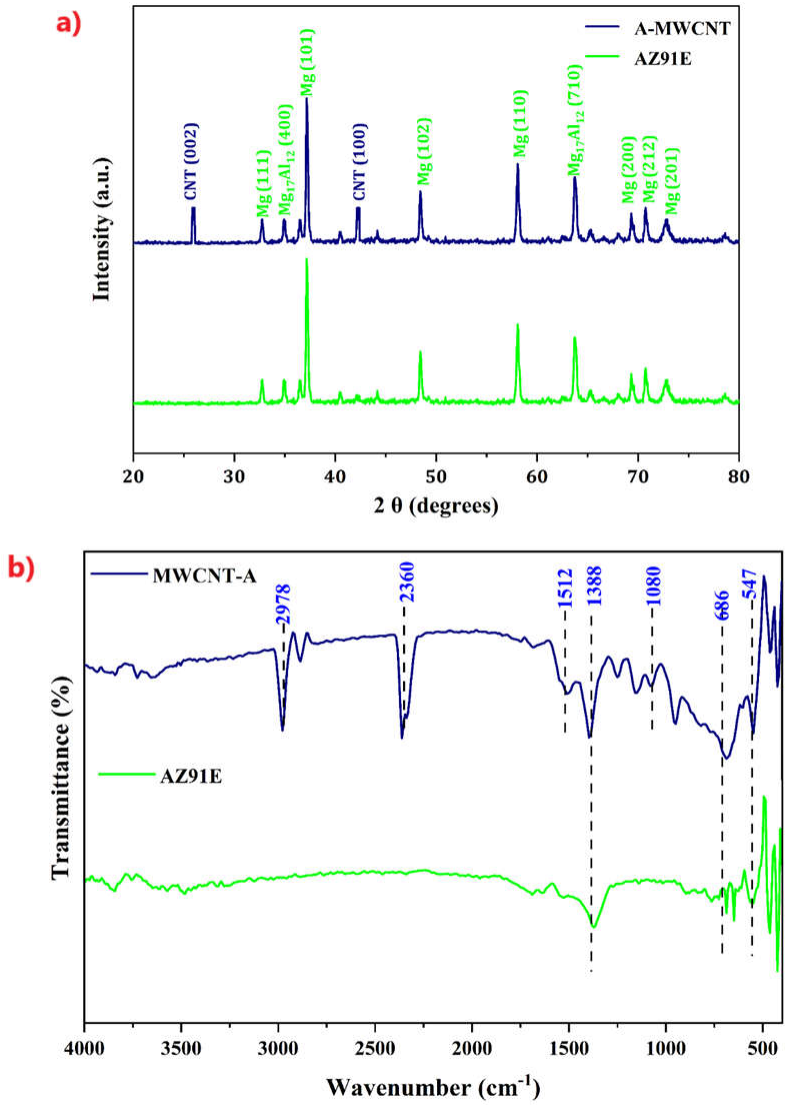

Figure 1. (a) XRD and (b) FTIR spectrum of prepared A-MWCNT and AZ91E samples.

The MWCNTs can introduce local stress concentrations at the interfaces between the nanotubes and the surrounding matrix. These stress concentrations can cause local deformations in the magnesium lattice near the MWCNT-matrix interfaces, resulting in microstrain. Additionally, during thermal cycling or exposure to elevated temperatures, differences in the coefficients of thermal enlargement between the MWCNTs and the Mg matrix can result in thermal mismatch stresses. These stresses can induce lattice distortions and microstrain near the MWCNTs. Thus, the observation of crystallographic and microstructural information from XRD data exhibits that the MWCNT has a noteworthy impact over the mechanical possessions of

AZ91E magnesium alloy, collectively contributing towards improving overall mechanical properties. Furthermore, the absence of additional peaks in the XRD spectrum depicts the structural purity of prepared samples and the lack of additional impurities.

Functional group analysis

The FTIR spectra of the pure MWCNT-casted magnesium alloy AZ91E offer valuable insights into the composite material's chemical composition and bonding characteristics which involves measuring the absorption of infrared radiation by the sample, enabling the identification of functional groups and molecular vibrations present in the material. Figure 1(b) shows that sharp peaks observed at the wavenumbers 2978 and 686 cm^{-1} can be attributed to surface-adsorbed water molecules from the atmosphere [15]. Furthermore, a shrill peak at 547 cm^{-1} corresponds to the metal bond of Mg in the magnesium alloy, while a narrow peak at 686 cm^{-1} and 1380 cm^{-1} indicates the existence of Al during the formation of the secondary phase. The C=C of the multi-walled carbon nanotube backbone is observed at 1512 cm^{-1} [16]. Additionally, stretching vibrations observed at 2360 and 1080 cm^{-1} are accompanying through C-C and C-O natures, corresponding to defects in the internal portion of MWCNT. The FTIR confirms the integration of MWCNT with AZ91E magnesium alloy, with the predominant existence of C=C, and C-O natures of MWCNT. Moreover, the absence of additional peaks in the FTIR spectra of the A-MWCNT sample indicates the absence of additional impurities, which is consistent with XRD findings [17, 18].

Morphological analysis

The SEM images of AZ91E, as seen in Figure 2(a), depict the smooth surface of allows. The morphology of the plate also shows minimal dents and defects on the material's surface. Additionally, the SEM images of MWCNT, as seen in Figure 2(c), revealed the distinctive tubular structure of MWCNTs, characterized by multiple concentric graphene layers arranged in cylindrical tubes. The images exhibited the nanotubes' elongated morphology with diameters typically ranging from a few nanometers to tens of nanometers. Additionally, SEM analysis allowed for the visualization of MWCNT bundles or agglomerates, which may occur due to van der Waals interactions between individual nanotubes. The observed surface defects, such as kinks, twists, and junctions, were also observed in the SEM images, highlighting the structural complexity of MWCNTs and serve as nucleation sites for grain refinement during solidification, leading to the formation of finer grains in the alloy microstructure.

Consequently, the dispersion of MWCNT to Mg alloy, the surface morphology of the magnesium alloy becomes more refined and homogeneous, with reduced grain size and improved mechanical properties. Additionally, MWCNTs can influence the nucleation and growth kinetics of various phases in the magnesium alloy, such as intermetallic or secondary phases. By promoting the formation of a more uniform distribution of these phases, MWCNTs contribute to developing a more stable and corrosion-resistant surface morphology. Moreover, the high surface area and aspect ratio of MWCNTs facilitate the formation of a robust interface between the nanotubes and the magnesium alloy matrix. This robust interface enhances the load transfer efficiency and improves the mechanical bonding between the MWCNTs and the alloy matrix, enhancing mechanical properties and surface morphology. As depicted in Figure 2(b), the EDX spectrum of AZ91E reveals a predominant composition of magnesium and aluminium, consistent with the alloy's specifications. Additionally, the existence of oxygen peaks in the spectrum indicates superficial oxidation of the alloy, a common phenomenon observed in magnesium-based materials exposed to atmospheric conditions. In contrast, the EDX spectrum of the MWCNTs demonstrates a higher weight percentage and atomic percentage of carbon, which is characteristic of the rolled carbon rings comprising the nanotube structure. The minimal oxygen peaks in the

MWCNT spectrum may arise from surface defects or impurities inherent to the nanotube fabrication process.

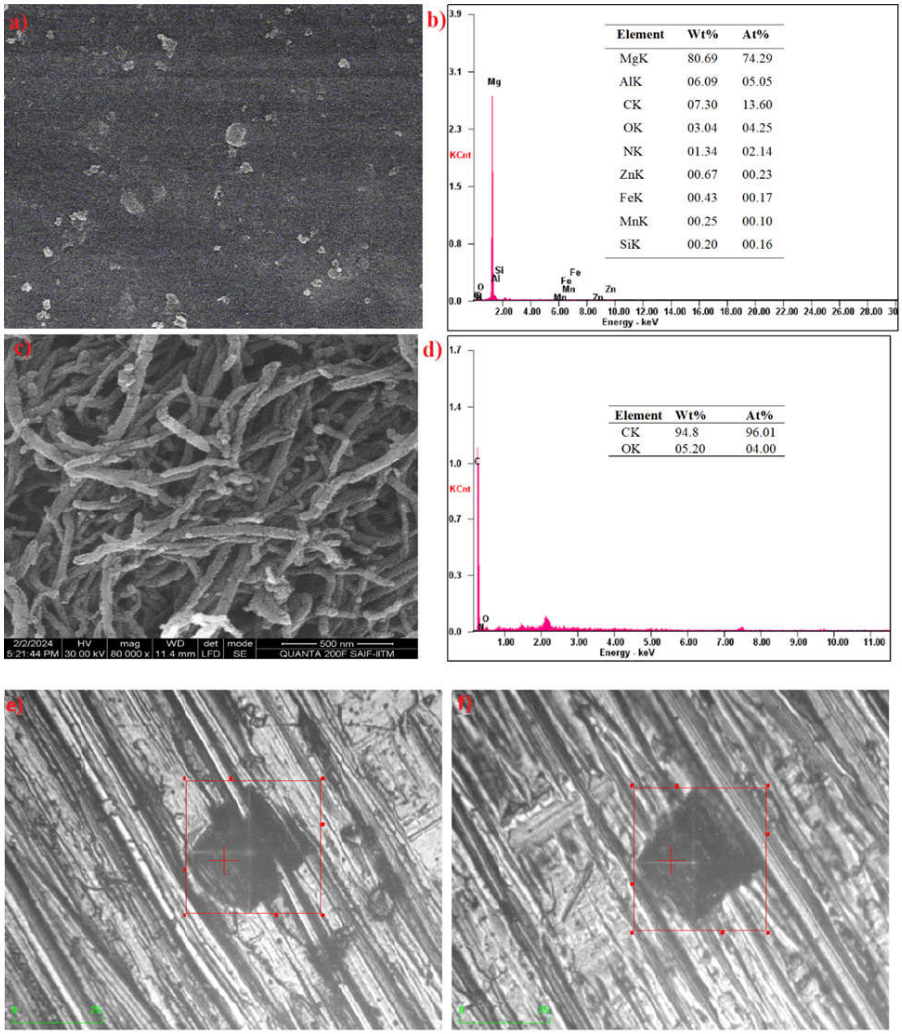

Figure 2. (a) SEM of AZ91E, (b) EDX of AZ91E, (c) SEM of MWCNT, (d) EDX of MWCNT, Vickers hardness impression of the diamond tip of (e) A-MWCNT and (f) AZ91E alloy samples.

Hardness analysis

To confirm the reproducibility and accuracy of the data, the Vickers hardness test was performed at five distinct sites on each sample. The Vickers hardness indenter was utilised to create impressions by exerting a regulated force into the material's surface, forming a square-shaped

indentation, as depicted in Figure 2(e and f). By conducting repeated tests at different points on the sample surface, any possible differences in hardness caused by variations in the microstructure or surface imperfections can be considered, resulting in a thorough evaluation of the material's mechanical properties. The Vickers hardness readings were subsequently averaged to derive a representative assessment for the prepared A-MWCNT and AZ91E alloy samples. The A-MWCNT sample exhibits a Vickers hardness value of 291.87, indicating robust hardness characteristics. Conversely, the AZ91E alloy sample demonstrates a lower hardness value of 61.855. This discrepancy in hardness values underscores the influence of composition and microstructural features on the mechanical performance of the materials. The higher hardness observed in the A-MWCNT sample can be attributed to the reinforcing effect of MWCNTs which enhance the alloy matrix's structural integrity, effectively resisting plastic deformation and increasing hardness. Additionally, MWCNTs can hinder dislocation movement within the crystal lattice, further contributing to the material's hardness. Further, MWCNTs form interfacial solid bonds with the magnesium matrix, resulting in efficient load transfer between the nanotubes and the surrounding material which helps to distribute applied loads more evenly throughout the alloy, contributing to its overall hardness. In contrast, the lower hardness observed in the AZ91E alloy sample can be attributed to its composition, primarily consisting of magnesium and aluminium as the magnesium alloys typically exhibit lower hardness than materials with more metallic constituents. Furthermore, the microstructural features of the AZ91E alloy, like grain size and phase distribution, may also contribute to its relatively lower hardness. The limited hardness drawback for magnesium alloys in variation application is significantly reduced with the casting employed with MWCNT. Additionally, higher hardness generally correlates with increased resistance to wear and abrasion. In corrosion environments where mechanical wear is a concern, such as in industrial and automobile settings, magnesium alloys with improved hardness can better withstand abrasive forces, reducing the likelihood of surface damage and corrosion initiation

Contact angle measurements

Contact angle measurement is crucial for understanding materials' wettability and surface energy. It helps us understand how materials interact with liquid phases and can be applied in industries, including coatings, adhesives, and corrosion protection. The contact angle measurements in this investigation showed notable disparities between A-MWCNT and AZ91E magnesium alloy surfaces. The measured contact angle of 123.65° for A-MWCNT indicates that the surface is Super-hydrophobic. Various variables, such as carbon nanotubes on the surface, can explain the hydrophobicity seen in A-MWCNT. The densely packed arrangement of nanotubes creates a tortuous path for the liquid, hindering its ability to wet the surface effectively which reduces the solid-liquid contact area and increases the contact angle, indicating improved hydrophobicity. Furthermore, the carbon nanotubes' chemical makeup and surface functional groups could reduce interactions with polar solvent molecules, resulting in a hydrophobic surface. Conversely, the contact angle of 44° observed for AZ91E indicates a relatively hydrophilic surface. The reduced contact angle found in AZ91E signifies a stronger attraction to the testing liquid, indicating higher surface energy and improved wetting behaviour compared to A-MWCNT. The hydrophilic properties of AZ91E can be explained by characteristics such as surface oxidation, the presence of alloying elements, and surface roughness. These factors enhance the ability of AZ91E to interact with polar solvent molecules and allow wetting.

The observed disparities in contact angle between A-MWCNT and AZ91E magnesium alloy surfaces emphasise the impact of surface shape, composition, and structure on wetting behaviour. Superhydrophobic surfaces are highly desirable in food storage and transportation applications for several reasons. Firstly, they facilitate the easy removal of water and other liquids from the surface, preventing the accumulation of moisture and reducing the risk of corrosion and microbial growth. Additionally, the repellent nature of superhydrophobic surfaces minimises the adhesion

of food particles, residues, and contaminants, helping to maintain cleanliness and hygiene standards. In practical terms, the super-hydrophobicity of the MWCNT-casted magnesium alloy can enhance the efficiency of food packaging, storage containers, and transportation equipment. Surfaces treated with MWCNTs can effectively repel liquids, including water, oils, and food juices, preventing them from permeating or damaging packaging materials and ensuring the integrity of food products during transit. Moreover, the superhydrophobic properties of the alloy contribute to its overall durability and longevity, as it reduces the likelihood of corrosion, fouling, and degradation over time. This extended service life translates to cost savings and improved reliability for food storage and transportation infrastructure.

Antibacterial activity

The biofouling control over alloys of prepared A-MWCNT and AZ91E samples were tested with the antibacterial assay against *Escherichia coli* and *Staphylococcus aureus* with 3 different concentrations such as 25, 50, and 100 µL. A-MWCNT and AZ91E have significant inhibition zones in contradiction of *E. coli* and *S. aureus*. It is also detected that with the rise of sample concentration, the antibacterial zone of inhibition has increased. Further, as seen in Table 1, the zone of inhibition of A-MWCNT is comparatively higher than the AZ91E. The enhanced zone of inhibition observed for A-MWCNT compared to AZ91E against both *E. coli* and *S. aureus* can be attributed to several factors inherent to the MWCNT incorporation in the magnesium alloy. Firstly, MWCNTs possess intrinsic antimicrobial properties due to their unique nanostructure and physicochemical characteristics. The high aspect ratio and large surface area of MWCNTs facilitate direct contact and interaction with bacterial cells, leading to physical disruption of the cell membrane and subsequent cell death. This direct antimicrobial effect of MWCNTs contributes to the broader zone of inhibition observed in A-MWCNT samples compared to pure AZ91E alloy [3]. Additionally, the existence of MWCNTs can alter the surface possessions of the magnesium alloy, creating an inhospitable environment for bacterial colonization and growth. Incorporating MWCNTs may modify the surface chemistry and topography of the alloy, making it less conducive to bacterial adhesion and biofilm formation. This alteration in surface characteristics inhibits the initial attachment of bacterial cells to the material surface, reducing the likelihood of biofilm formation and subsequent bacterial proliferation. Furthermore, MWCNTs can exert a synergistic antimicrobial effect when combined with the inherent antimicrobial properties of magnesium. Combining MWCNTs and magnesium alloy may release antimicrobial ions, such as magnesium ions, from the alloy surface. These ions can further inhibit bacterial growth and viability, enhancing the overall antimicrobial efficacy of A-MWCNT samples compared to AZ91E alloy alone.

The antibacterial activity mechanism of both A-MWCNT and AZ91E samples involves multifaceted interactions between the material surfaces and bacterial cells, inhibiting bacterial growth and viability [17]. For A-MWCNT samples, MWCNTs play a crucial role in the antibacterial activity mechanism which possess intrinsic antimicrobial properties attributed to their unique nanostructure and physicochemical characteristics and physically disrupt the bacterial cell membrane through various mechanisms when in contact with bacterial cells. The high aspect ratio and large surface area of MWCNTs enable direct interaction with bacterial cells, leading to mechanical puncturing or piercing of the cell membrane. This disruption compromises the bacterial cell's structural integrity, causing cellular content leakage and cell death. Additionally, the sharp edges and rough surface morphology of MWCNTs may further contribute to their antimicrobial activity by facilitating physical damage to bacterial cells upon contact. Furthermore, the presence of MWCNTs on the exterior of the Mg alloy can create a hostile microenvironment for bacterial colonization and growth.

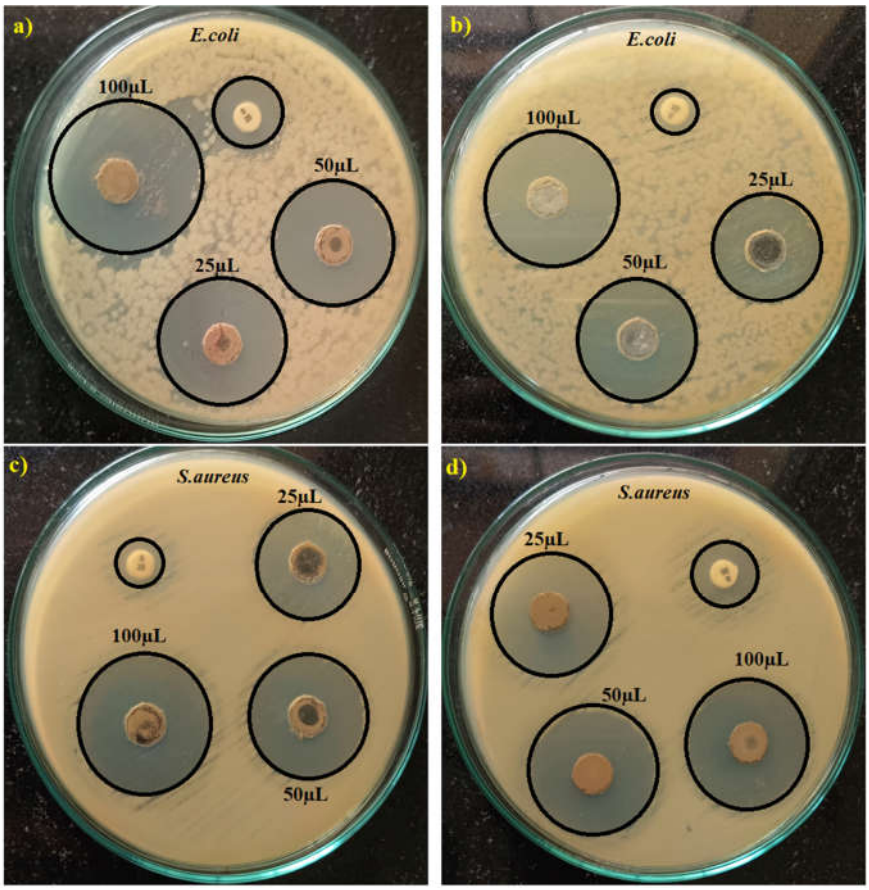

Figure 3. Antibacterial activity against *E. coli* (a) A-MWCNT and (b) AZ91E and *S. aureus (*c) A-MWCNT and (d) AZ91E.

The altered surface chemistry and topography of A-MWCNT samples may hinder bacterial adhesion and biofilm formation, preventing the initial attachment of bacterial cells to the material surface. This reduction in bacterial attachment limits the formation of biofilms, which are protective matrices produced by bacteria for enhanced survival and proliferation. A-MWCNT samples effectively inhibit bacterial growth and colonisation by disrupting bacterial attachment and biofilm formation. In contrast, AZ91E magnesium alloy exhibits antibacterial activity, albeit somewhat less than A-MWCNT samples. The antibacterial mechanism of AZ91E alloy is primarily ascribed to the proclamation of magnesium ions (Mg^{2+}) from the alloy surface. When in contact with aqueous environments, such as biological fluids or bacterial culture media, magnesium ions are released from the surface of AZ91E alloy through corrosion processes which can interact with bacterial cells and disrupt essential cellular processes, leading to bacterial cell death. Magnesium ions can interfere with bacterial membrane integrity, disrupt enzyme function, and induce oxidative stress within bacterial cells, ultimately resulting in antibacterial effects.

Table 1. Antibacterial zone of inhibition of prepared A-MWCNT and AZ91E samples.

Sample	Name of the bacteria							
	Staphylococcus aureus				*Escherichia coli*			
Concentration	Std	25	50	100	Std	25	50	100
A-MWCNT	9	29	33	41	17	32	38	51
AZ91E	18	28	31	38	12	29	33	42

Both A-MWCNT and AZ91E samples exhibit antibacterial activity through distinct mechanisms. While A-MWCNT samples primarily rely on the direct physical interaction and disruption of bacterial cells by MWCNTs, AZ91E samples leverage the proclamation of Mg ions from the alloy surface to inhibit bacterial growth and viability. The antibacterial activity of the MWCNT-casted magnesium alloy offers several advantages for food storage and transportation applications. Firstly, it helps to mitigate the risk of bacterial contamination during the handling, packaging, and transportation of food products, thereby reducing the incidence of foodborne illnesses and ensuring consumer safety. By inhibiting the growth and proliferation of pathogenic bacteria, the alloy contributes to the preservation of food quality which extends the shelf life of perishable goods.

Corrosion studies

As seen in Figure 4, the impedance frequency response analysis (FRA) spectra Nyquist plots obtained for AZ91E magnesium alloy and MWCNT-doped AZ91E magnesium alloy, immersed in varying concentrations of HCl electrolyte (1 M, 2 M, and 3 M), revealed intriguing insights into the corrosion behaviour of the materials. The Nyquist plots display the fundamental part of impedance (Z') against the imaginary part (Z") in a semicircular pattern. The impedance spectra were characterised by linear lines, indicating a single time constant in the system. These linear lines signify a simplified electrochemical process, which is ascribed to the uniform corrosion behaviour of the Mg alloys in the HCl electrolyte. At lower concentrations of HCl (1 M), the Nyquist plots exhibited relatively smaller diameters of the semicircular arcs for AZ91E magnesium alloy and MWCNT-doped AZ91E magnesium alloy. This suggests lower charge transfer resistance and enhanced ion mobility, reflecting an initial stage of corrosion [17]. As the concentration of HCl increased to 2 M and 3 M, the diameter (d) of the hemispherical arcs in the Nyquist conspiracies expanded, indicating an increase in charge transfer resistance and a reduction in ion mobility. This phenomenon is attributed to the intensification of the corrosive environment, leading to accelerated corrosion rates and decreased corrosion resistance of the magnesium alloys. Furthermore, the impedance spectra for the MWCNT doped AZ91E magnesium alloy displayed smaller semicircular arcs than the undoped AZ91E alloy at all concentrations of HCl electrolyte. This observation suggests that incorporating MWCNTs improves corrosion resistance in the magnesium alloy, potentially due to forming a protective barrier layer or modifying the alloy's surface properties.

Tafel plots serve as critical tools in analysing the corrosion behaviour of materials, particularly in this study of AZ91E magnesium alloy and MWCNT doped magnesium alloy under varying concentrations of HCL electrolyte. By constructing Tafel plots, researchers can illuminate the electrochemical corrosion kinetics of these alloys, shedding light on their behaviour under different environmental conditions. The plots depict the relationship between the current density (log j) logarithm and electrode potential (E), offering valuable insights into the electrochemical processes governing corrosion kinetics. The observed linear relationship between log j and E in the Tafel plots indicates adherence to Tafel's law, where corrosion rates are proportional to the overpotential. Furthermore, the slopes of the Tafel plots provide information about corrosion kinetics, with steeper slopes suggesting higher corrosion rates and shallower slopes indicating

reduced corrosion rates. As seen in Figure 5, the Tafel relation reveals that the MWCNT-doped sample (A-MWCNT) exhibits a drift towards the positive potential direction, indicating a higher corrosion inhibition rate than the AZ91E sample. However, an intriguing observation emerges as the concentration of HCl electrolyte increases from 1 M to 3 M. This leads to a significant decrease in corrosion inhibition rate, as seen in Table 2. The solution's heightened concentration of chloride ions competes with the inhibitor molecules, displacing them and reducing their effectiveness in forming a protective barrier against corrosion. Despite this, the corrosion rate of A-MWCNT remains minimal, even at high HCl concentrations compared to the AZ91E plate. This phenomenon can be ascribed to the capability of MWCNTs to develop a physical barrier on the surface of Mg alloy, impeding the penetration of corrosive species such as chloride ions. This barrier layer acts as a protective shield, effectively preventing direct contact between the alloy surface and corrosive environments, thus showcasing the potential of MWCNT doping in enhancing corrosion resistance.

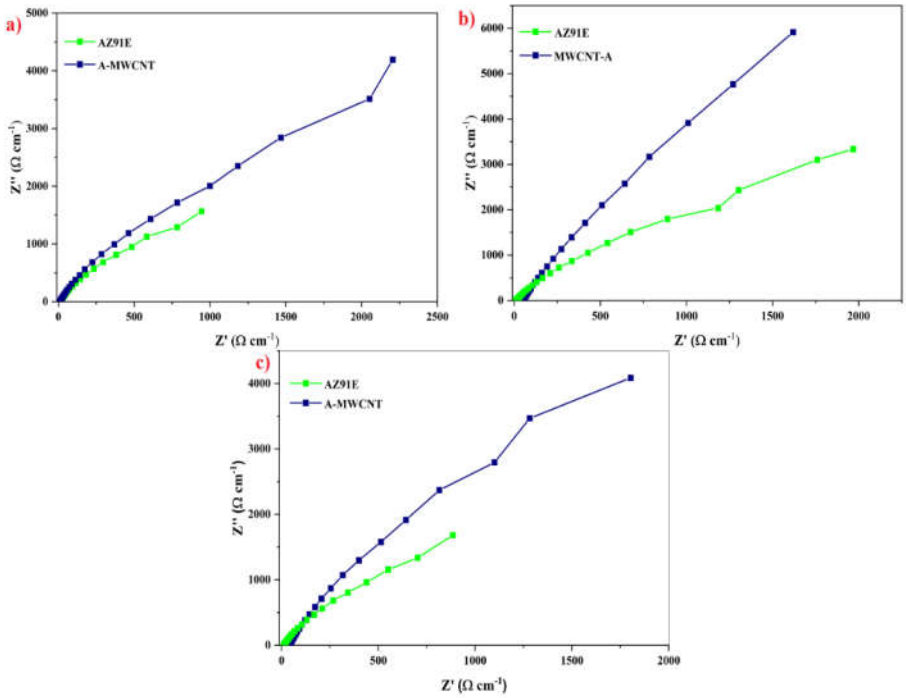

Figure 4. Nyquist plot for prepared AZ91E and A-MWCNT sample at (a) 1 M, (b) 2 M, and (c) 3 M of the HCl electrolyte.

The Bode phase angle plot in Figure 6 illustrates that the phase angle is depicted on the y-axis, while the logarithm of frequency is represented on the x-axis for the MWCNT-infused magnesium alloy (A-MWCNT) and the pure magnesium alloy AZ91E. The phase angle provides valuable information about the phase relationship between a system's input and output signals. In the electrochemical impedance spectroscopy context, the phase angle is particularly insightful as it reflects the phase shift between the applied voltage signal and the resulting current response across different frequencies. In Figure 6, the phase angle plot reveals characteristic trends and features associated with the electrochemical behaviour of the materials under investigation. The phase

angle approaches 90º at low frequencies, indicating capacitive behaviour dominant in this frequency range. Capacitive processes typically involve charge storage and release at the electrode-electrolyte interface, leading to a phase shift between the voltage and current signals. As the frequency increases, the phase angle gradually decreases towards zero degrees. This decrease suggests a transition from capacitive to resistive behaviour, where the phase relationship between the voltage and current becomes more aligned. In the intermediate frequency range, the phase angle may exhibit fluctuations or peaks, reflecting the presence of specific electrochemical processes or time constants within the system. Furthermore, comparing the phase angle plots of A-MWCNT and AZ91E allows for insights into the differences in their electrochemical behaviour. A higher phase angle magnitude for A-MWCNT than AZ91E may indicate enhanced capacitive behaviour or a more pronounced protective effect of the MWCNT infusion on the magnesium alloy.

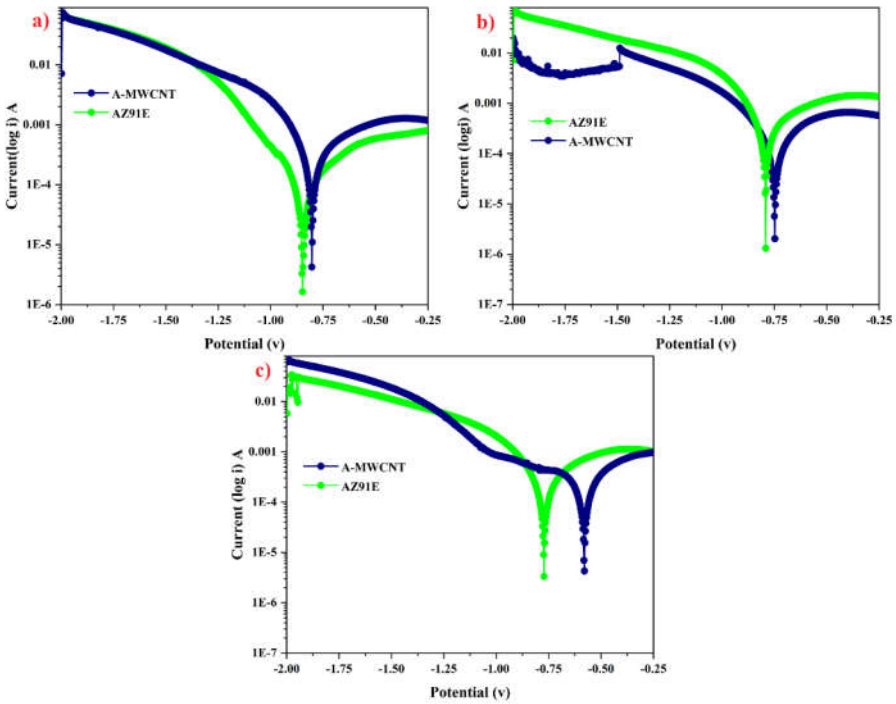

Figure 5. Tafel plot for prepared AZ91E and A-MWCNT sample at (a) 1 M, (b) 2 M, and (c) 3 M HCl electrolyte.

The phase angle, logarithm of impedance (log Z), and logarithm of frequency (log f) relationships between A-MWCNT and pure magnesium alloy AZ91E are shown in this Bode figure as well. Figure 6 shows the solution and protective layer ohmic resistances (Rs) as a function of frequency. Here you can see the region that the working electrode and reference electrode encompass. Both the phase angle and the logarithmic magnitude of impedance (Z) fall to zero at 1000 Hz, which is indicative of the solution's resistive properties and their relationship to resistance. A negative-sloped linear equation around -1 in the middle frequency bands indicates a direct and proportional relationship between frequency and the logarithm of the absolute

impedance value. This equation provides more evidence that the relationship is proportional. As the phase angle becomes larger, the system under study begins to behave capacitively. There can be only one time constant if the Bode plot has a single peak. The phase angle diagram's solitary peak provides the necessary context. If the Bode phase diagram values for A-MWCNT are somewhat higher than AZ91E, it might indicate that the protective layer is more resilient. In electrochemical processes, the low-frequency regions represent the first step. Capacitive action causes an increase in impedance magnitude in certain areas. The impedance signal may show an increase in amplitude and phase angle due to slower ion movement to and from the electrode surface, which might be produced by diffusion-limited processes. The corrosion resistance of A-MWCNT is superior than that of pure AZ91E, according to impedance and phase angle measurements. Therefore, mild steel plates are better protected from corrosion when made of magnesium alloys that include MWCNTs infused into them rather than pure magnesium alloys.

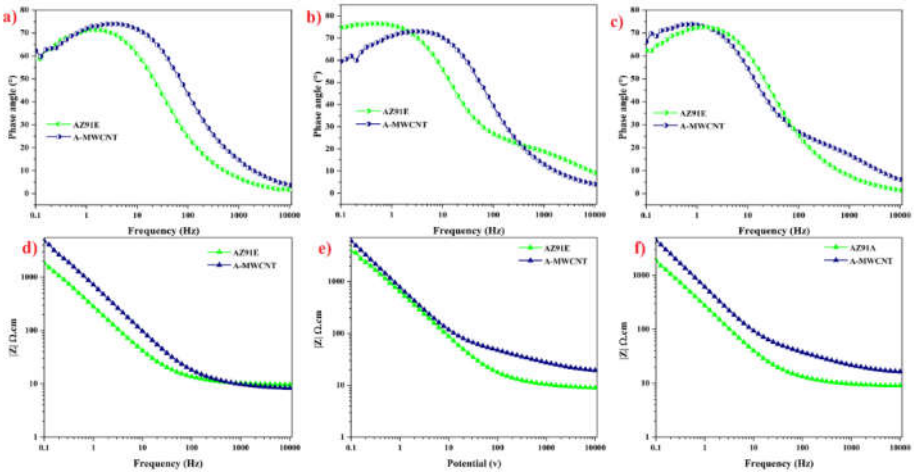

Figure 6. Phase angle plot for prepared AZ91E and A-MWCNT sample at (a) 1 M, (b) 2 M, and (c) 3 M of the HCl electrolyte and phase resistance plot at (d) 1 M, (e) 2 M, and (f) 3 M HCl electrolyte.

The displacement-load curve obtained from nanoindentation provides crucial insights into the mechanical characteristics of both A-MWCNT and AZ91E alloy samples. Figure 7 illustrates the curve representing the relationship between the applied load and the resulting displacement during the indentation process after electrochemical analysis with several volume of HCl electrolyte. In the case of A-MWCNT, the displacement-load curve displays distinct features indicative of the material's response to mechanical loading. Initially, as the load is applied, the displacement increases gradually with minimal resistance, indicating elastic deformation behaviour. This phase corresponds to the elastic regime, where the material undergoes reversible deformation, reflecting its ability to recover its original shape upon removal of the load. However, upon surpassing a critical load threshold, the displacement experiences a sudden increase, signaling the onset of plastic deformation which marks the initiation of irreversible plasticity within the material, characterized by permanent deformation. The slope of the curve during this plastic deformation phase reflects the material's hardness, representing its resistance to plastic deformation. Conversely, the displacement-load curve for the AZ91E alloy sample exhibits similar trends but with notable distinctions.

Table 2. The corrosion parameters for the prepared A-MWCNT and AZ91E alloys.

Electrolyte	Samples	E_{corr} ($\mu A/cm^2$)	I_{corr} ($\mu A/cm^2$)	Polarisation confrontation	Rate of corrosion (mm/year)
1 M HCl	A-MWCNT	-0.848	0.0205	562.91	0.23894
	AZ91E	-0.745	1.91	316.11	2.2294
2 M HCl	A-MWCNT	-0.803	1.523	162.43	1.7677
	AZ91E	-0.776	3.8	199.93	4.444
3 M HCl	A-MWCNT	-0.79	2.04	138.4	2.375
	AZ91E	-0.58	6.7	221.2	7.794

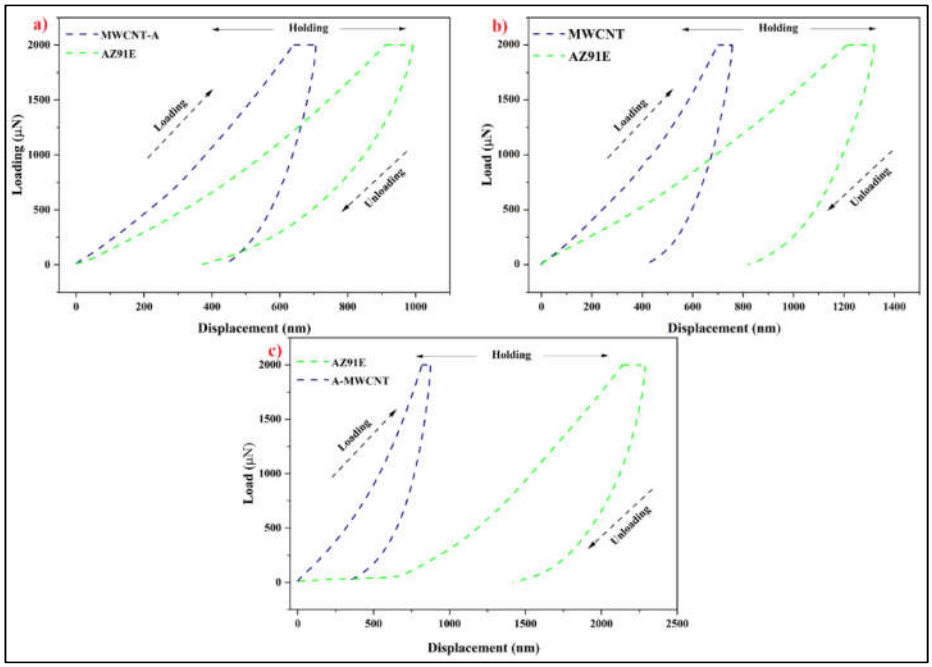

Figure 7. Nanoindentation curve obtained for prepared A-MWCNT and AZ91E at (a) 1 M, (b) 2 M, and (c) 3 M HCl electrolyte.

The absence of MWCNTs in the AZ91E alloy results in a mechanical response different from the A-MWCNT sample. The curve may show differences in the elastic and plastic deformation regimes due to the distinct microstructure and composition of the AZ91E alloy. Without the reinforcement provided by MWCNTs, the AZ91E alloy may demonstrate different hardness levels and resistance to plastic deformation. Furthermore, adding MWCNTs introduces nanoscale features and reinforcement mechanisms that augment the mechanical possessions of the A-MWCNT sample. The presence of MWCNTs can lead to improved hardness, strength, and toughness, contributing to the overall mechanical performance of the alloy. Additionally, the interaction between MWCNTs and the magnesium matrix may influence the composite material's deformation behaviour and mechanical response.

Table 3. Topographical parameters for prepared MWCNT and AZ91E alloys.

Name of the electrolyte	Name of the samples	Depth displacement (max.) (h) nm	Surface roughness (Ra) (nm) at the corrosion area	
			Before	After
1 M HCl	A-MWCNT	60.25	57.258	61.22
	AZ91E	99.23	83.47	93.22
2M HCl	A-MWCNT	101.25	65.98	72.33
	AZ91E	152.42	101.22	121.25
3 M HCl	A-MWCNT	126.07	83.28	91.67
	AZ91E	213.21	149.29	163.87

As seen in Table 3, there is a noteworthy rise in the average surface roughness (Ra); this can be attributed to forming an oxide layer of magnesium alloys when subjected to electrochemical analysis. However, the A-MWCNT sample has shown a minimal increase in surface roughness, which is ascribed to MWCNT creating a defending barrier layer on the surface of the magnesium alloy. The nanotubes possess a high aspect ratio and nanoscale size, enabling them to envelop the alloy's surface adequately. This creates a physical barrier that successfully protects the alloy from corrosive damage. The barrier layer prevents the entry of acidic substances, such as ions and moisture that cause corrosion and create surface irregularities.

Moreover, the exceptional anticorrosion properties of MWCNT-casted magnesium alloy offer robust protection against corrosion-induced degradation in corrosive environments commonly encountered in food processing facilities. The material demonstrates resilience against varying concentrations of HCl, a corrosive agent often used in food processing, ensuring the longevity and reliability of equipment and infrastructure vital for food storage and transportation operations. Furthermore, the antibacterial activity exhibited by MWCNT-doped magnesium alloy is crucial for maintaining food safety and quality during storage and transportation. By efficiently constraining the development of bacteria like *E. coli* as well as *S. aureus*, the material helps to mitigate the risk of microbial contamination, ensuring the integrity and wholesomeness of food products throughout the supply chain. The incorporation of MWCNT into magnesium alloy also enhances its mechanical properties, as evidenced by increased Vickers hardness, which improves the durability and wear resistance of components used in food storage and transportation equipment. Additionally, the superhydrophobic nature of the MWCNT-casted magnesium alloy surface contributes to the prevention of moisture ingress, facilitating the safe and hygienic storage and transportation of food products by minimizing the risk of contamination and spoilage.

CONCLUSION

The successful preparation of MWCNT-casted magnesium alloy through the stir casting technique underscores a simple and cost-efficient process for enhancing the properties of magnesium-based materials. Analysis of the microstructural properties using XRD reveals significant alterations in strain and dislocation within the magnesium alloy, indicative of the structural modifications induced by the incorporation of MWCNTs. Furthermore, the contact angle measurements demonstrate the superhydrophobic nature of the MWCNT-casted magnesium alloy surface, highlighting the profound influence of MWCNTs on surface properties and potential applications in environmental remediation. Moreover, the corrosion protection the prepared MWCNT-casted magnesium alloy offers against various concentrations of HCl electrolyte underscores its high corrosion inhibition activity compared to pure magnesium alloy counterparts. This enhanced corrosion resistance is crucial for applications in corrosive environments, such as marine or industrial settings, where prolonged service life and durability are paramount. Additionally, the antibacterial activity exhibited by the MWCNT-casted magnesium alloy showcases its efficacy in combating biofouling-induced alloy deterioration, addressing environmental concerns associated

with microbial contamination and material degradation. The alloy maintains its structural integrity and performance over extended periods by mitigating biofouling effects, contributing to environmental sustainability and resource conservation.

REFERENCES

1. Luo, A.A. Recent magnesium alloy development for elevated temperature applications. *Int. Mater. Rev.* **2004**, 49, 13–30.
2. Easton, M.; Beer, A.; Barnett, M.; Davies, C.; Dunlop, G.; Durandet, Y.; Blacket, S.; Hilditch, T.; Beggs, P. Magnesium alloy applications in automative structures. *J. Met.* **2008**, 60, 57–62.
3. Mondolfo, L.F. Structure of the aluminium : magnesium : zinc alloys. *Metall. Rev.* **1971**, 16, 95–124.
4. Zeng, R.; Rong-chang, Z.; Jin, Z.; Wei-jiu, H.; Dietzel, W.; Kainer, K.U.; Blawert, C.; Wei, K.; Fki, J. Review of studies on corrosion of magnesium alloys. *Trans. Nonferrous Met.* **2006**, 16, 763–771.
5. Gusieva, K.; Davies, C.H.J.; Scully, J.R.; Birbilis, N. Corrosion of magnesium alloys: The role of alloying. *Int. Mater. Rev.* **2015**, 60, 169–194.
6. Song, G.; Bowles, A. Corrosion resistance of aged die cast magnesium alloy AZ91D. *Mater. Sci. Forum.* **2003**, 1044, 73–79.
7. Song, G. Recent progress in corrosion and protection of magnesium alloys. *Adv. Eng. Mater.* **2005**, 7, 563–586.
8. Ghali, E.; Dietzel, W.; Kainer, K.U. General and localized corrosion of magnesium alloys: A critical review. *J. Mater. Eng. Perform.* **2004**, 13, 7–23.
9. Hoche, H.; Scheerer, H.; Probst, D. Development of a plasma surface treatment for magnesium alloys to ensure sufficient wear and corrosion resistance. *Surf. Coat. Int.* **2003**, 174, 1018–1023.
10. Veronica, V.; Fernando, C.; Diego, S.; Adelina, S. Graphene and PANI functionalization with myristic acid for incorporation in anti-corrosion epoxy coatings. *Prog. Org. Coat.* **2022**, 172, 107146.
11. Fahad, M. Tribological and ageing behavior of Az91D magnesium alloy fortified with nano lanthanum and nanoceria by stir casting for aviation application. *Ind. Lubr. Tribol.* **2021**, 73, 635–641.
12. Dargusch, M.S.; Bowles, A.L.; Pettersen, K.; Bakke, P.; Dunlop, G.L. The effect of silicon content on the microstruture and creep behavior in die-cast magnesium as alloys. *Metall Mater Trans A.* **2004**, 35A, 1905–1909.
13. Tang, A.; Pan, F.; Yang, M.; Transactions, R.C.M. Mechanical properties and microstructure of magnesium-aluminum based alloys containing strontium. *Mater. Trans.* **2008**, 49, 1203–1211.
14. Zeng, X.; Wang, Y.; Ding, W.; Luo, A.A.; Sachdev, A.K. Effect of strontium on the microstructure, mechanical properties, and fracture behavior of AZ31 magnesium alloy. *Metall Mater Trans A.* **2006**, 37, 1333–1341.
15. Kubasek, J.; Vojtech, D.; Mater, I.P. Structural and corrosion characterization of biodegradable Mg-Zn alloy castings. *Kovove. Mater.* **2012**, 50, 415–424.
16. Mahadevaiah, R.; Lalithamba, H.S.; Shekarappa, S.; Hanumanaika, R. Synthesis of Nα-protected formamides from amino acids using MgO nano catalyst: Study of molecular docking and antibacterial activity. *Scientia Iranica* **2017**, 24, 3002–3013.
17. Lin, C.P.; Shu, C.M.; Chou, Y.C.; Hsieh, T.F.; Hsieh, Y.C.; Shu, C.M.; Chou, Y.C.; Shu, C.M.; Hsieh, T.F.; Hsieh, Y.C. Comparisons of MWCNTs and acidified process by HNO_3 on thermal stability by DSC and TG-FTIR. *J. Therm. Anal. Calorim.* **2010**, 123, 641–646.
18. Avid, A.; Jafari, S. Surface modification of MWCNT and its influence on properties of paraffin/MWCNT nanocomposites as phase change material. *J. Appl. Polym. Sci.* **2020**, 137, 48428.